



# Heterogeneous Photocatalysis with Niobium Doped-Titanium Substrates Treated by Plasma Electrolytic Oxidation

Fábio R. Orsetti<sup>a</sup>, Thaís M. Gonçalves<sup>a</sup>, Lívia Sottovia<sup>a</sup>, Elaine B. Figueiredo<sup>b</sup>, Ana M. Ferrari<sup>b\*</sup> ,  
Elidiane C. Rangel<sup>a</sup>, Nilson C. Cruz<sup>a</sup> 

<sup>a</sup>Universidade Estadual Paulista (UNESP), Laboratório de Plasmas Tecnológicos, Sorocaba, SP, Brasil.

<sup>b</sup>Universidade Tecnológica Federal do Paraná (UTFPR), Apucarana, PR, Brasil.

Received: September 01, 2022; Revised: October 06, 2022; Accepted: October 19, 2022

Plasma Electrolytic Oxidation (PEO) was employed for the generation of porous niobium-containing surfaces with enhanced photocatalytic activity. Pulses of 500 and 600 V, with a repetition rate of 60 Hz, were applied to titanium disks immersed in niobium-containing electrolytic solutions. The treatment time ranged from 180 to 600 s, and the surface morphology was analyzed by scanning electron microscopy, while X-ray diffraction was employed in the evaluation of crystallographic structure. The optical gap of the samples was determined from UV-Vis reflection spectra, and an automated goniometer was used for contact angle and surface energy measurements. More than 35% of Nb has been incorporated into the samples. Under certain conditions, the treatments resulted in a reduction of the optical gap from 3.18 to 2.63 eV as compared to as-received samples. Photocatalytic degradation rates of methylene blue as high as 70% have been reached after 120 minutes under irradiation with UV-Vis light.

**Keywords:** Photocatalytic activity, titanium, niobium oxide, plasma electrolytic oxidation, PEO.

## 1. Introduction

One of the major concerns in modern society is the contamination of water through chemical fertilizers, agrochemicals, pesticides, oil, dyes, heavy metals, drugs, and hormones. Worldwide, industries are the largest responsible for pollution, being responsible for more than half the volume of contaminated water<sup>1-3</sup>.

There are many processes and technologies available for water treatment. Physical and chemical methods generally include using anion exchange resins, flotation, ozonation, biodegradation, nanofiltration, electrolysis, irradiation, adsorption, filtration, and the use of activated carbon<sup>1-4</sup>. In addition, there are also biological processes that are less expensive and waste less energy compared to physical and chemical processes, but they require longer treatment times. In industries, physical and chemical operations are not widely deployed due to high toxicity and costs<sup>1</sup>.

The traditional degradation of pollutants in some circumstances, such as pesticides and dyes degradation, has shown to be ineffective or excessively time-consuming<sup>2</sup>. In this context, Advanced Oxidative Processes (AOPs) appear as a promising alternative solution. AOPs have as their main characteristic the generation of strongly oxidizing free radicals that can degrade the organic structures of the contaminants, resulting in CO<sub>2</sub>, H<sub>2</sub>O, and nontoxic byproducts<sup>2</sup>. Particularly important and commonly used, the hydroxyl radicals can be produced by several methods, including the catalytic decomposition of H<sub>2</sub>O<sub>2</sub> in acid environment (through reactions such as Fenton or photo-Fenton) and reactions involving ozone (O<sub>3</sub>) or semiconductors, such as

TiO<sub>2</sub> and ZnO, typically under ultraviolet irradiation (UV)<sup>1</sup>. In this way, the AOPs can be classified as homogeneous systems with irradiation (combining O<sub>3</sub> and UV, H<sub>2</sub>O<sub>2</sub> and UV, or H<sub>2</sub>O<sub>2</sub> and ultrasound, for instance), homogeneous systems without radiation (combining O<sub>3</sub> and H<sub>2</sub>O<sub>2</sub>, O<sub>3</sub> and OH<sup>-</sup>, or H<sub>2</sub>O<sub>2</sub> and Fe<sup>2+</sup> (Fenton reaction)), heterogeneous systems with irradiation (TiO<sub>2</sub>/O<sub>2</sub>/UV or TiO<sub>2</sub>/H<sub>2</sub>O<sub>2</sub>/UV), and heterogeneous systems without irradiation (such as the electron-Fenton reaction)<sup>5</sup>.

In the last decades, the search for more economical processes for removing organic contaminants led to the development of heterogeneous photocatalysis, an efficient AOP for the degradation and mineralization of pollutants in water<sup>3-5</sup>. In this process, the organic compound is mineralized to water, carbon dioxide, and inorganic salts, in the presence of a photocatalyst semiconductor, a light source, and an oxidizing agent (i.e., oxygen)<sup>6</sup>.

The efficiency of photocatalysis depends on the semiconductor properties, such as crystalline structure, surface area, porosity, and optical gap<sup>6</sup>. Titanium dioxide (TiO<sub>2</sub>) is one of the most used semiconductors in water purification by heterogeneous photocatalysis. Specifically, anatase crystalline form presents high efficiency, low cost, photostability, and absence of toxicity, among other factors<sup>6-9</sup>.

Studies conducted in the 1990s have shown that the addition of niobium in small amounts has increased the photocatalytic efficiency, selectivity, and chemical stability of TiO<sub>2</sub>. Thereafter, an increasing interest in using such element has been observed, especially in the form of niobium oxides, since the combination of niobium with other semiconductors results in unique properties,

\*e-mail: [anamferrari@utfpr.edu.br](mailto:anamferrari@utfpr.edu.br)

such as reduced optical bandgap, for instance. Recently, Hu et al.<sup>10</sup> have evaluated the photoelectric properties of intrinsic TiO<sub>2</sub> and different concentrations of Nb-doped with TiO<sub>2</sub> using density functional theory. Zhang et al.<sup>11</sup> assessed the degradation of methyl orange using Nb-doped TiO<sub>2</sub> thick films and concluded that the improvement in photocatalytic performance was greatly attributed to the dominated crystalline orientation of the (0 0 1) plane for Nb-doped TiO<sub>2</sub>. Nogueira et al.<sup>12</sup> observed that the presence of Nb in the crystal structure of TiO<sub>2</sub> increased the photoactivity of the powders compared to unmodified TiO<sub>2</sub> powders. It was proved that the introduction of NiO into TiO<sub>2</sub> led to the formation of p–n heterojunctions, improving the separation of electron-hole pairs and photocatalytic activity<sup>13</sup>.

It is interesting to point out that, despite some increment in the photoactivity of TiO<sub>2</sub>, all the works mentioned above have used TiO<sub>2</sub> in the form of powder, which requires additional processes to retrieve the catalyst after the pollutant degradation. Therefore, continuous, not powdered, semiconductors with large surface area are very attractive candidates to enhance the efficiency of the heterogeneous photocatalysis process.

In this context, Plasma Electrolytic Oxidation (PEO), is an up-and-coming technology because it allows the production of highly porous coatings with variable chemical compositions<sup>14</sup>. PEO has some characteristics like conventional anodization. Both processes are based on the application of a voltage between two electrodes immersed in an electrolytic solution, being one of them the sample to be treated. However, the voltages employed in the PEO are substantially higher than those used in anodization. When the voltage is low, the surface of the sample is covered by an oxide film similar to that one produced in conventional anodizing. However, as the voltage increases, intense electric fields can be established through the insulating oxide layer. On those spots where such electric fields exceed the dielectric strength of the coating, tiny electric arcs, generally referred to as micro-arcs, are formed increasing the temperature locally to thousands of degrees<sup>15,16</sup>. The heating so generated can continuously melt the coating and substrate, resulting in the formation of pores and chemical reactions involving species on the surface and in the electrolyte. In this way, the coatings can be formed containing elements of the substrate, the oxide layer, and the electrolyte. Furthermore, as the modification of treatment characteristics, such as the compositions of the electrolyte and the substrate, and the applied voltage, influences the chemical reactions and the intensity of the micro-arcs, the modification of process parameters enables the tailoring of the properties of the coatings to best match the requirements of a given application.

In this work, plasma electrolytic oxidation has been applied to produce high porous niobium-doped titanium surfaces. It has been investigated the influence of the treatments on the improvement of the photocatalytic degradation of organic compounds.

## 2. Materials and Methods

Grade 2 titanium samples 9.6 mm in diameter were sandpapered to a mirror-like finishing. The samples were sonicated in deionized water and 99.8% isopropyl alcohol baths for 480 s in each liquid. After cleaning, the samples

were dried with a hot air gun. The electrolytic solution has been prepared diluting either 5.0 g or 10.0 g of ammonium niobium oxalate (ANO, NH<sub>4</sub>NbO(C<sub>2</sub>O<sub>4</sub>)<sub>2</sub>), kindly supplied by CBMM, Brazilian Metallurgy and Mining Company, in one liter of distilled water. Each treatment was performed using 330 ml of fresh solution.

PEO treatments were performed in a water-cooled stainless-steel vessel as previously described by Orsetti et al.<sup>17</sup>, using a pulsed bipolar voltage source (MAO 30, Plasma Technology LTD).

As summarized in Table 1, pulses of 500 (the minimum voltage to observe the formation of microarcs) and 600 V (the highest voltage to avoid cracks and fissures on the coatings) at a repetition rate of 60 Hz with 60% duty cycles, have been applied to the samples during 180, 480 and 600 s. During the treatments the average current density ranged from 2.1 to 0.14 A/cm<sup>2</sup>.

The morphology the coatings obtained by PEO and the pristine substrate were evaluated by scanning electron microscopy (SEM) using a JEOL JSM 6010 electron microscope. For contact angle measurements and surface energy calculations, it has been used an automated goniometer (Rame-Hart 100-00) with water and diiodomethane as probe liquids. Coatings crystalline structure were investigated by X-ray diffraction in a Panalytical – X'Pert PRO MPD diffractometer with a copper cathode operated at 45 kV and 40 mA with incident beam at 5°, scanning from 20° to 90° with a 0.05° pitch resulting in 1 second per step. Identification of peaks was performed using X'Pert Pro Highscore Software, and the International Centre for Diffraction Data (ICDD) database. The optical bandgap of the treated samples and pristine substrate were determined from reflectance UV-Vis spectra collected by a PerkinElmer Lambda 750 spectrophotometer coupled to an integrating sphere. The spectra obtained from diffuse reflectance (%R) were analyzed by Tauc plot method<sup>18</sup>, as given in Equation 1

$$\frac{1}{(h\nu\alpha)^n} = A(h\nu - E_g) \quad (1)$$

where,  $h$  is the Planck constant,  $\nu$  is the frequency of light,  $\alpha$  is the absorption coefficient,  $E_g$  is the energy gap and  $A$  is constant.

The value of  $n$  is related to the sample natural transitions<sup>19</sup>. For amorphous film or indirect bandgap, the most used value is  $n = \frac{1}{2}$ . In direct gap the most usual value is  $n = 2$ . Only in special situations (direct transition prohibited by symmetry) the value is  $n = \frac{3}{2}$ . It is important to emphasize that indirect

**Table 1.** Treatment parameters used in preparation of niobium containing titanium samples by PEO.

Sample	Voltage (V)	Time (s)	ANO concentration (g L <sup>-1</sup> )
A1	500	180	10.0
A2	500	480	10.0
A3	500	600	10.0
A4	500	600	5.0
A5	600	600	5.0

transitions can occur simultaneously with direct transitions. However, they cannot be detected in absorption spectra due to their low probability<sup>20</sup>.

The spectra of diffuse reflectance were converted to the Kubelka-Munk function  $F(R)$ . That is,  $\alpha$  in Equation 1 is replaced by  $F(R)$ , giving rise to Equation 2:

$$(F(R)hv)^{\frac{1}{n}} = A(hv - E_g) \quad (2)$$

In this way,  $E_g$  can be obtained from the plot of  $(F(R)hv)^{\frac{1}{n}}$  versus  $hv$ . The bandgap energy can be found at the intersection of a line tangent to the linear part of the graph and the energy axis<sup>18-21</sup>. It has been adopted  $n = \frac{1}{2}$  in this study.

To evaluate the photocatalytic degradation of organic compounds, 5.0 mg / L aqueous solution of cationic dye methylene blue ( $MB^+$ ,  $C_{16}H_{18}ClN_3S$ , molecular mass 319.85 g.mol<sup>-1</sup>) was used as the pollutant model. The radiation source was a 125 W- UV/Vis mercury lamp without the glass bulb to maximize the UV/Vis emission fitted 5 cm apart from the samples, which resulted in an illumination density of about 0.4 W/cm<sup>2</sup>. The lamp emission spectra have been previously reported<sup>21</sup>. The reaction time was 120 minutes and for each analysis, 20 mL of methylene blue solution and five samples were used. The samples were kept in a Petri dish under mechanical stirring. The fraction of dye degradation,  $C/C_0$ , Equation 3, were obtained from measurements of initial and final absorbance,  $Abs_{initial}$  and  $Abs_{final}$ , respectively, of the solution at 655 nm (with molar absorptivity of  $9.6 \times 10^4$  L mol<sup>-1</sup>cm<sup>-1</sup>):

$$\%degradation = \frac{c}{c_0} = \frac{Abs_{initial} - Abs_{final}}{Abs_{initial}} * 100 \quad (3)$$

### 3. Results and Discussion

#### 3.1. Morphology, composition, and thickness

The SEM micrographs of the samples produced using 10.0 g L<sup>-1</sup> of ammonium niobium oxalate (ANO) with different treatment times are shown in Figures 1a-c. As can be observed in Figure 1a, the sample treated for 180 s exhibits a slightly coarse surface. In addition, from the cross-section SEM micrograph presented in the inset, it is possible to verify that a dense, roughly  $2.6 \pm 1.1$   $\mu$ m thick- layer has been grown. Completely different microstructures were formed when the treatment time was increased. Highly porous hierarchical structures can be observed in the micrographs of the samples treated during 480 and 600 s, Figure 1b and Figure 1c, respectively. To understand such observations, one should keep in mind that the treatments result in the growth of insulating layers, whose thicknesses increase as the treatment time is increased, on the substrate. Consequently, if the treatment time is too short, the dielectric strength of the coating may not be high enough to develop intense electric fields through the layers. In such a case, the micro arcs, resulting from the electric breakdown of the coating, are not intense enough to reach the substrate causing the formation of large pores<sup>22</sup>. As the coatings' thickness increases, the microarcs become more and more intense, and the resulting local heating can punctually melt the substrate, forming pores and increasing the rates of

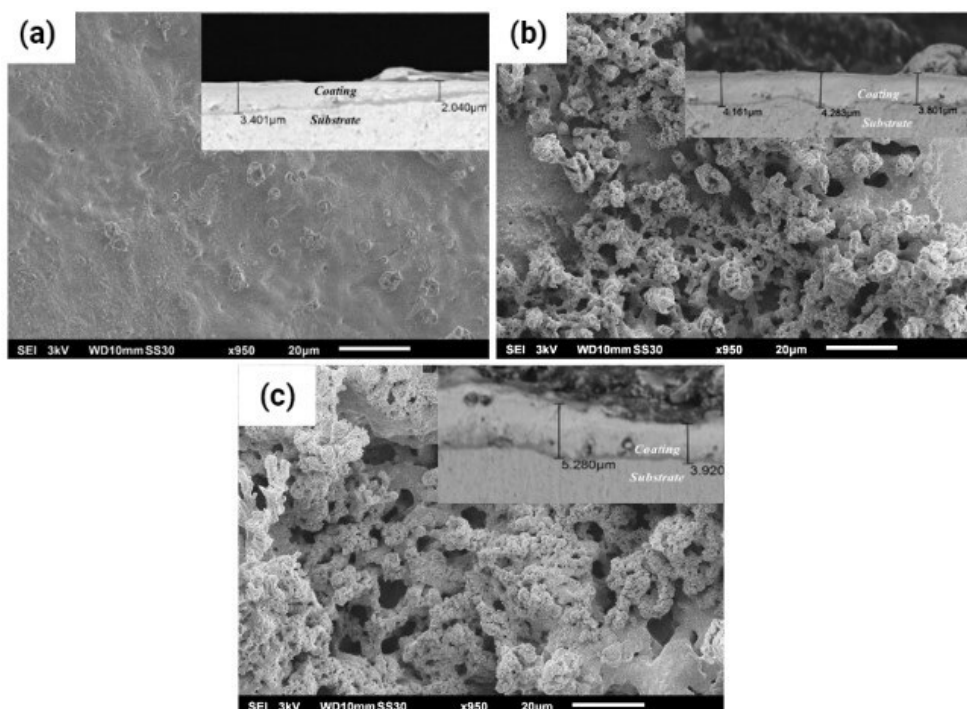


**Figure 1.** Scanning electron micrographs of the samples treated by PEO using 10 g L<sup>-1</sup> of ANO, 500 V and different treatment times: (a) 180 s, (b) 480 s, and (c) 600 s. The insets present the respective cross-section micrographs.

chemical reactions occurring near or on the surface<sup>23</sup>. In this way, the coating growth mechanism involves the formation of pores through the melting of the substrate, the re-deposition of the molten metal quenched by the electrolyte, and the incorporation of species through reactions involving species on the surface and in the electrolyte. Such suppositions are corroborated by a deeper analysis of the micrographs shown in Figures 1b and 1c. Comparing the pictures, it is possible to observe that the higher the treatment time, the thicker the coatings (as highlighted by the onset cross-section SEM micrographs). Furthermore, pores and the clustered structures on the surface of the sample treated for 600 s are present in larger density and with larger diameters than those observed on the samples subjected to shorter treatments. Therefore, the results suggest that increasing the treatment time up to 600 s results in samples with larger surface area, which contributes to the enhancement of the photocatalytic activity.

As it can be concluded from Figure 2, which presents the proportion of the elements as determined by EDS on the whole area of the SEM micrographs, niobium has been effectively incorporated into the samples in proportions ranging from 31% to 36% as the treatment time was increased from 180 to 600 s. In addition, titanium is only observed on the

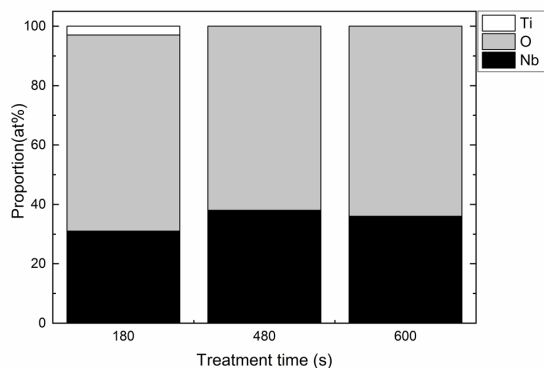


**Figure 2.** Proportion of the elements detected by EDS on samples treated by PEO using  $10 \text{ g L}^{-1}$  of ANO, 500 V and different treatment times.

samples treated for up to 180 s, which indicates that, after a certain treatment time, the coating grows mostly by reactions involving species in the electrolyte rather than the melting and redeposition of species on the substrate.

Figures 3a and 3b present the SEM micrographs of the samples produced using  $5.0 \text{ g L}^{-1}$  of ANO. As it can be noticed, the reduction of the concentration of the oxalate resulted in smoother coatings in comparison with those obtained with  $10 \text{ g L}^{-1}$ . Even though the coating thickness increased from  $1.39 \pm 0.14 \mu\text{m}$  to  $2.75 \pm 0.18 \mu\text{m}$  when the voltage was increased from 500 V to 600 V, both coatings are thinner than that grown with  $10 \text{ g L}^{-1}$  during 600 s that is  $5.50 \pm 1.71 \mu\text{m}$  thick, as it can be inferred from Figure 1c. Furthermore, titanium has been detected by EDS in proportions of 10% and 6% on the samples treated using 500 V and 600 V, respectively, and the proportion of Nb incorporated to the coatings was only ~60% of the amount detected on the samples treated using  $10 \text{ g L}^{-1}$  of ANO. Together, these results, which agree with the previous discussions, can be understood considering that, in this case, the incorporation of species and, consequently, the coating growth is limited by the reduced availability of reagents.

Although increasing the voltage from 500 V to 600 V roughly doubled the thickness of the coating, cracks can be observed on the surface of the sample grown under the highest voltage, Figure 3b. Such defects are consequences of the establishment of high thermal power micro arcs, which are deleterious to the coating integrity<sup>23</sup>. Therefore, higher voltages are disadvantageous for the growing of the high-quality porous coatings pursued in this work.

### 3.2. Wettability and surface energy

Considering that the pollutants to be degraded are mostly dispersed in water, completely wettable surfaces are highly desired. In this sense, water contact angle measurements revealed that all the samples, with the exception of the pristine titanium and the sample treated for 600 s using  $5 \text{ g L}^{-1}$  of ANO and 500 V (sample A4), are fully wettable, with null contact angles. The values of water contact angle and surface energy and its polar and dispersive components of Ti and the sample A4 are presented in Table 2. As suggested by the polar component of surface energy, a possible explanation

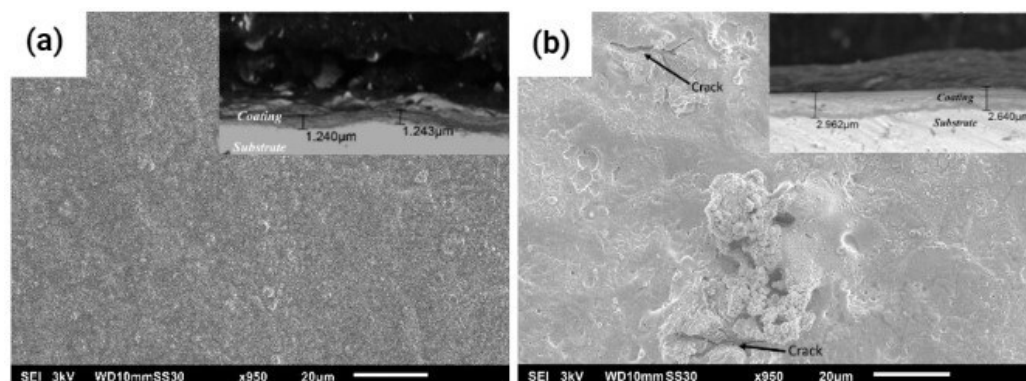


**Figure 3.** SEM micrographs of samples treated by PEO using  $5 \text{ g L}^{-1}$  of ANO for 600 s at (a) 500 V and (b) 600 V. The insets present the respective cross-section micrographs.

**Table 2.** Water contact angle, surface energy ( $E_s$ ), and its polar ( $\gamma_p$ ) and dispersive ( $\gamma_D$ ) components of as-received and PEO treated titanium samples.

Sample	Contact angle (°)	$\gamma_P$ (Dyn cm <sup>-1</sup> )	$\gamma_D$ (Dyn cm <sup>-1</sup> )	ES (Dyn cm <sup>-1</sup> )
Pristine Ti	66.7	7.3	45.4	52.7
A4	81.9	2.9	39.3	42.2

for the observation that sample A4 is less hydrophilic than untreated Ti can be the fact that the surface of that sample is less polar than that of the metal.

### 3.3. X-ray diffraction

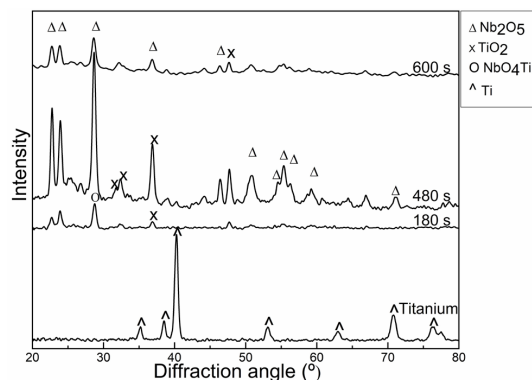
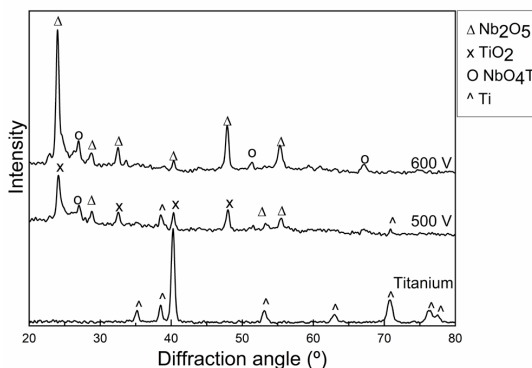
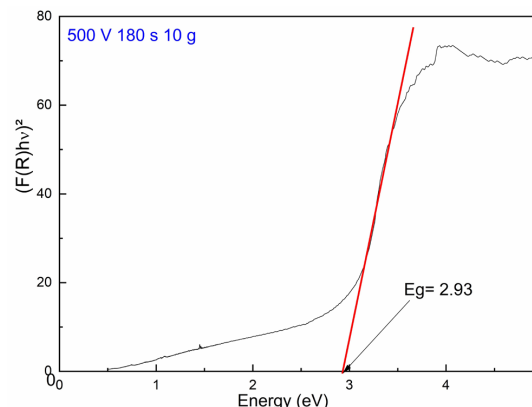
The X-ray diffractograms of titanium samples as-received and after treatments with 10 g L<sup>-1</sup> of ANO are shown in Figure 4. Peaks ascribed to metallic titanium and both niobium and niobium-titanium oxides are observed on the diffractogram of the sample treated for 180 s. When the treatment time was increased to 480 s, it was noticed an increase in the number of peaks ascribed to niobium oxide. Finally, a clear predominance of peaks associated to niobium oxide is observed on the diffractogram of the sample treated during 600 s.

The diffractograms of the coatings produced using 5.0 g L<sup>-1</sup> of ANO and pristine Ti are shown in Figure 5. Most of the peaks on the diffractogram of sample A4 are ascribed to anatase and titanium. In addition, niobium oxide was also observed with a minor contribution. When the voltage was increased to 600 V, it revealed the formation of both niobium and niobium-titanium oxides, which is an interesting fact, as such oxides may result in bandgap reduction.

### 3.4. Ultraviolet- visible diffuse reflectance spectroscopy

The optical bandgap,  $E_g$ , of the samples were obtained from the linear coefficient of lines tangent to the linear region of the plots of  $(F(R)hv)^2$  versus  $hv$ , as illustrated in Figure 6 for the sample treated for 180 s at 500 V using 10 g L<sup>-1</sup> of ANO. All the results are summarized in Table 3. A bandgap of 3.18 eV was obtained for the native oxide layer on the untreated sample, which is very close to 3.2 eV that is usually reported in the literature as the  $E_g$  of TiO<sub>2</sub> in anatase phase<sup>24,25</sup>.

From the results, one can note that the bandgaps of those samples that presented peaks ascribed to NbO<sub>4</sub>Ti on their x-ray diffractograms (samples A1, A4, and A5) are substantially lower than the  $E_g$  of the other samples. Therefore, it can be inferred from the results that all the treatments caused the reduction of bandgap in comparison to the as-received titanium, confirming the initial premise of this work that the incorporation of niobium would reduce the bandgap. As the optical bandgap of pure niobium oxide is about 3.4 eV<sup>26</sup>, such reduction can be understood considering the addition of an element on the group V-B of the periodic table to a semiconductor from an element on the group IV-B, giving rise to *n*-type semiconductors. The energy levels added to the band structure in the presence of impurities and dopants cause the displacement of Fermi levels towards the conduction band, facilitating the excitation<sup>27</sup>. It is interesting to point out that the values of  $E_g$  obtained in this work are significantly lower than those reported in the literature for

**Figure 4.** X-ray diffractograms of titanium samples as-received and after treated by PEO with 10 g L<sup>-1</sup> of ammonium niobium oxalate, 500 V and different treatment times.**Figure 5.** X-ray diffractograms of pristine titanium and samples treated by PEO with 5.0 g L<sup>-1</sup> of ammonium niobium oxalate, for 600 s and different voltages.**Figure 6.** Illustration of Tauc's plot using Kubelka-Munk function for the determination of optical bandgaps from reflectance spectra.

**Table 3.** Optical bandgap of samples treated by PEO according to conditions given in Table 3.

Sample	Eg(eV)
A1	2.93
A2	3.01
A3	3.01
A4	2.84
A5	2.63

TiO<sub>2</sub>-containing surfaces<sup>24-26</sup>. The lowest bandgap (2.63 eV) caused the absorption edge of the material to shift from 390 nm to 470 nm, that is, from UV to blue light.

### 3.5. Photocatalytic activity

Figure 7 shows the variation of the relative concentration ( $C/C_0$ ) of methylene blue (MB) solution as a function of time under UV/Vis radiation. A photolysis test was carried out to evaluate the effect of the lighting alone on the variation of dye concentration. Such test revealed that about 8% of the dye was degraded by the light after 120 min of illumination. The photodegradation rate with untreated titanium samples was slightly higher than the photolysis.

After 120 minutes, the dye concentration was reduced by 12%. The sample A5 resulted in photodegradation of 10% after 15 min of illumination. After 120 min of irradiation, the concentration of MB was reduced by 30%, revealing that, even with the lowest bandgap (2.63 eV) obtained in this work, this sample does not show significant photocatalytic activity. Slightly better performances have been observed with samples A1 and A4, which presented very similar photodegradation rates (approximately 15% after 15 min and 35% after 120 min of exposure). Both samples had relatively smooth surfaces and bandgaps smaller than untreated titanium.

Among all the evaluated samples, sample A3 presented the highest photocatalytic activity, reducing by about 55% the concentration of the dye after only 30 min of illumination. After 120 minutes, 70% of the dye was degraded. Therefore, thicker coatings with larger amounts of niobium oxide are supposed to present larger photocatalytic activity. It is important to recall that, as it is well known, defects associated with the presence of oxygen are fundamental in the photocatalytic process for inhibiting electron/hole recombination. The reduction potential of niobium pentoxide is high enough to transfer electrons from its conduction band to oxygen molecules generating structural defects. Oxygen vacancies on the surface act as trappers of photoinduced charges and adsorption sites as well where the charge can be transferred to the adsorbed compounds to be degraded, preventing electron/hole recombination, and, thus, increasing the photocatalytic activity<sup>28</sup>. Many times, comparisons among the photocatalytic degradation rates obtained by different authors are not straightforward as they depend on several parameters such as light intensity, the distance between the light source and the solution, volume, and concentration of dye solution, etc. Even though it is possible to situate our results in relation to others in literature. While here we have degraded 70% of the dye in 120 minutes, Yin et al.<sup>29</sup> have used Nb-doped TiO<sub>2</sub> produced by a sol-gel technique, and the highest degradation rate

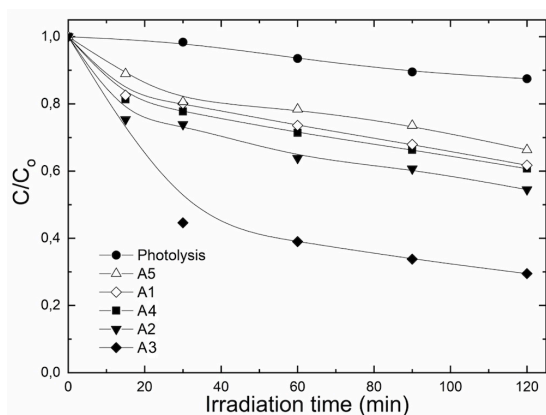


**Figure 7.** Relative concentration ( $C/C_0$ ) of methylene blue solution as a function of time under UV/Vis irradiation in contact with different samples.

they have attained was 65% after 240 minutes, which was even smaller than the degradation observed with pure TiO<sub>2</sub>. Using TiO<sub>2</sub> and Nb for the synthesis of Nb-doped titanate nanostructures, Byun et al.<sup>30</sup> have observed the performance of the nanostructures in the degradation of Methylene Blue and Rhodamine B was significantly higher than those resulting from pure TiO<sub>2</sub>. The photocatalytic activity of Nb-doped titanate nanostructures was 1.4 times and 3.1 times higher for Methylene Blue and Rhodamine B, respectively. Yang et al.<sup>31</sup> studied the photocatalytic activity of Nb-TiO<sub>2</sub> films and observed a significant improvement in the photocatalytic activity of doped films compared to TiO<sub>2</sub> films. After 120 minutes of irradiation, about 70% of Rhodamine B was degraded using Nb-TiO<sub>2</sub> thin film.

## 4. Conclusions

Niobium has effectively been incorporated to titanium surfaces by plasma electrolytic oxidation. It has been observed that both surface morphology and composition can be adjusted through the variation of the treatment parameters. By changing electrolyte composition and exposure time, it is possible to produce smoother or more porous surfaces with crystalline structures ranging from predominantly niobium oxide to more complex compositions including anatase and mixed titanium niobium oxide. From cross-section micrographs it has been observed that longer treatments resulted in thicker coatings. All the treatments reduced the optical bandgap as compared to the value determined from untreated titanium. In particular, the treatment for 600 s with 600 V and 5 gL<sup>-1</sup> of ammoniacal niobium oxalate resulted in the largest bandgap reduction, reaching 2.63 eV. The treatment for 600 s using 500 V and 10 gL<sup>-1</sup> of ANO produced the thickest and roughest sample, which also presented the best photocatalytic activity. With this sample, degradation of 70% of methylene blue has been achieved after UV/Vis irradiation for 120 minutes.

## 5. Acknowledgments

The authors would like to thank Brazilian sponsoring agencies FAPESP (Proc. 2015/03159-6) and CNPq for financial support.

## 6. References

1. Chaleshtori MZ, Hosseini M, Edalatpour R, Masud SS, Chianelli RR. New porous titanium-niobium oxide for photocatalytic degradation of bromocresol green dye in aqueous solution. *Mater Res Bull.* 2013;48(10):3961-7.
2. Ohtani B. Photocatalysis A to Z: what we know and what we do not know in a scientific sense. *J Photochem Photobiol Photochem Rev.* 2010;11(4):157-78.
3. Saupe GB, Zhao Y, Bang J, Yesu NR, Carballo GA, Ordóñez R, et al. Evaluation of a new porous titanium-niobium mixed oxide for photocatalytic water decontamination. *Microchem J.* 2005;81(1):156-62.
4. Bukman L, Fernandes-Machado NR, Caetano W, Tessaro AL, Hioka N. Treatment of wastewater contaminated with ionic dyes: liquid-liquid extraction induced by reversed micelle followed by photodegradation. *Separ Purif Tech.* 2017;189:162-9.
5. Huang CP, Dong C, Tang Z. Advanced chemical oxidation: its present role and potential future in hazardous waste treatment. *Waste Manag.* 1993;13(5-7):361-77.
6. Marković S, Rajić V, Stanković A, Veselinović L, Belošević-Cavor J, Batalović K, et al. Effect of PEO molecular weight on sunlight induced photocatalytic activity of ZnO/PEO composites. *Sol Energy.* 2016;127:124-35.
7. Ibadon AO, Fitzpatrick P. Heterogeneous photocatalysis: recent advances and applications. *Catalysts.* 2013;3(1):189-218.
8. Borges ME, Sierra M, Cuevas E, García RD, Esparza P. Photocatalysis with solar energy: sunlight-responsive photocatalyst based on TiO<sub>2</sub> loaded on a natural material for wastewater treatment. *Sol Energy.* 2016;135:527-35.
9. Herrmann JM, Duchamp C, Karkmaz M, Hoai BT, Lachheb H, Puzenat E, et al. Environmental green chemistry as defined by photocatalysis. *J Hazard Mater.* 2007;146(3):624-9.
10. Hu Y, Li L, Zhang Z, Gao S, Guo J, Yang P. Improving photoelectric properties by using Nb-doping on TiO<sub>2</sub>. *Chem Phys Lett.* 2022;803:139830.
11. Zhang C, Uchikoshi T, Ishigaki T. Effect of crystalline orientation on photocatalytic performance for Nb-doped TiO<sub>2</sub> nanoparticles. *Adv Powder Technol.* 2021;32(11):4149-54.
12. Nogueira MV, Lustosa GMMM, Kobayakawa Y, Kogler W, Ruiz M, Monteiro ES Fo, et al. Nb-doped TiO<sub>2</sub> photocatalysts used to reduction of CO<sub>2</sub> to methanol. *Adv Mater Sci Eng.* 2018;2018:7326240.
13. Mannaa MA, Qasim KF, Alshorifi FT, El-Bahy SM, Salama RS. Role of NiO nanoparticles in enhancing structure properties of TiO<sub>2</sub> and its applications in photodegradation and hydrogen evolution. *ACS Omega.* 2021;6(45):30386-400.
14. Gupta P, Tenhundfeld G, Daigle EO, Ryabkov D. Electrolytic plasma technology: science and engineering: an overview. *Surf Coat Tech.* 2007;201(21):8746-60.
15. Dunleavy CS, Golosnoy IO, Curran JA, Clyne TW. Characterisation of discharge events during plasma electrolytic oxidation. *Surf Coat Tech.* 2009;203(22):3410-9.
16. Klappkiv MD. State of an electrolytic plasma in the process of synthesis of oxides based on aluminum. *Mater Sci.* 1996;31(4):494-9.
17. Orsetti FR, Bukman L, Santos JS, Nagay BE, Rangel EC, Cruz NC. Methylene blue and metformin photocatalytic activity of CeO<sub>2</sub>-Nb<sub>2</sub>O<sub>5</sub> coatings is dependent on the treatment time of plasma electrolytic oxidation on titanium. *Applied Surface Science Advances.* 2021;6:100143.
18. Ebraheem S, El-Saied A. Band gap determination from diffuse reflectance measurements of irradiated lead borate glass system doped with TiO<sub>2</sub> by using diffuse reflectance technique. *Mater Sci Appl.* 2013;4(5):324-9.
19. Fujishima A, Zhang X, Tryk DA. TiO<sub>2</sub> photocatalysis and related surface phenomena. *Surf Sci Rep.* 2008;63(12):515-82.
20. López R, Gómez R. Band-gap energy estimation from diffuse reflectance measurements on sol-gel and commercial TiO<sub>2</sub>: a comparative study. *J Sol-Gel Sci Technol.* 2012;61(1):1-7.
21. Ferrari-Lima AM, Marques RG, Fernandes-Machado NRC, Gimenes ML. Photodegradation of petrol station wastewater after coagulation/flocculation with tannin-based coagulant. *Catal Today.* 2013;209:79-83.
22. Stojadinović S, Radić N, Vasilčić R, Petković M, Stefanov P, Zeković L, et al. Photocatalytic properties of TiO<sub>2</sub>/WO<sub>3</sub> coatings formed by plasma electrolytic oxidation of titanium in 12-tungstosilicic acid. *Appl Catal B.* 2012;126:334-41.
23. Antônio CA, Cruz NC, Rangel EC, Rangel RCC, Araujo TDES, Durrant SF, et al. Hydroxyapatite coating deposited on grade 4 Titanium by Plasma Electrolytic Oxidation. *Mater Res.* 2014;17(6):1427-33.
24. Wang Y, Zhu L, Wang M, Zhang M, Yang Y, Zhu Q, et al. Microstructure and photocatalytic activity of porous TiO<sub>2</sub>-Fe<sub>2</sub>O<sub>3</sub> composite film by PEO coupled with post heat treatment. *Int J Hydrogen Energy.* 2016;41(35):15703-9.
25. He J, Luo Q, Cai QZ, Li XW, Zhang DQ. Microstructure and photocatalytic properties of WO<sub>3</sub>/TiO<sub>2</sub> composite films by plasma electrolytic oxidation. *Mater Chem Phys.* 2011;129(1-2):242-8.
26. Furukawa S, Ohno Y, Shishido T, Teramura K, Tanaka T. Selective amine oxidation using Nb<sub>2</sub>O<sub>5</sub> photocatalyst and O<sub>2</sub>. *ACS Catal.* 2011;1(10):1150-3.
27. Callister WD, Rethwisch DG. *Materials science and engineering: an introduction.* 8th ed. New York: Wiley; 2010.
28. Tan H, Zhao Z, Zhu WB, Coker EN, Li B, Zheng M, et al. Oxygen vacancy enhanced photocatalytic activity of perovskite SrTiO<sub>3</sub>. *ACS Appl Mater Interfaces.* 2014;6(21):19184-90.
29. Yin M, Liu X, Hu L, Xu L, He J. Effects of Nb doping on microstructure and photocatalytic properties of TiO<sub>2</sub> thin film. *Desalination Water Treat.* 2016;57(15):6910-5.
30. Byun JM, Choi HR, Kim YD, Sekino T, Kim SH. Photocatalytic activity under UV/Visible light range of Nb-doped titanate nanostructures synthesized with Nb oxide. *Appl Surf Sci.* 2017;415:126-31.
31. Yang X, Min Y, Li S, Wang D, Mei Z, Liang J, et al. Conductive Nb-doped TiO<sub>2</sub> thin films with whole visible absorption to degrade pollutants. *Catal Sci Technol.* 2018;8(5):1357-65.